

# Disruption of $\text{Ca}^{2+}$ Homeostasis and Connexin 43 Hemichannel Function in the Right Ventricle Precedes Overt Arrhythmogenic Cardiomyopathy in Plakophilin-2–Deficient Mice

**BACKGROUND:** Plakophilin-2 (PKP2) is classically defined as a desmosomal protein. Mutations in PKP2 associate with most cases of gene-positive arrhythmogenic right ventricular cardiomyopathy. A better understanding of PKP2 cardiac biology can help elucidate the mechanisms underlying arrhythmic and cardiomyopathic events consequent to PKP2 deficiency. Here, we sought to capture early molecular/cellular events that can act as nascent arrhythmic/cardiomyopathic substrates.

**METHODS:** We used multiple imaging, biochemical and high-resolution mass spectrometry methods to study functional/structural properties of cells/tissues derived from cardiomyocyte-specific, tamoxifen-activated, PKP2 knockout mice (PKP2cKO) 14 days post-tamoxifen injection, a time point preceding overt electrical or structural phenotypes. Myocytes from right or left ventricular free wall were studied separately.

**RESULTS:** Most properties of PKP2cKO left ventricular myocytes were not different from control; in contrast, PKP2cKO right ventricular (RV) myocytes showed increased amplitude and duration of  $\text{Ca}^{2+}$  transients, increased  $\text{Ca}^{2+}$  in the cytoplasm and sarcoplasmic reticulum, increased frequency of spontaneous  $\text{Ca}^{2+}$  release events (sparks) even at comparable sarcoplasmic reticulum load, and dynamic  $\text{Ca}^{2+}$  accumulation in mitochondria. We also observed early- and delayed-after transients in RV myocytes and heightened susceptibility to arrhythmias in Langendorff-perfused hearts. In addition, ryanodine receptor 2 in PKP2cKO-RV cells presented enhanced  $\text{Ca}^{2+}$  sensitivity and preferential phosphorylation in a domain known to modulate  $\text{Ca}^{2+}$  gating. RNAseq at 14 days post-tamoxifen showed no relevant difference in transcript abundance between RV and left ventricle, neither in control nor in PKP2cKO cells. Instead, we found an RV-predominant increase in membrane permeability that can permit  $\text{Ca}^{2+}$  entry into the cell. Connexin 43 ablation mitigated the membrane permeability increase, accumulation of cytoplasmic  $\text{Ca}^{2+}$ , increased frequency of sparks and early stages of RV dysfunction. Connexin 43 hemichannel block with GAP19 normalized  $[\text{Ca}^{2+}]_i$  homeostasis. Similarly, protein kinase C inhibition normalized spark frequency at comparable sarcoplasmic reticulum load levels.

**CONCLUSIONS:** Loss of PKP2 creates an RV-predominant arrhythmogenic substrate ( $\text{Ca}^{2+}$  dysregulation) that precedes the cardiomyopathy; this is, at least in part, mediated by a Connexin 43-dependent membrane conduit and repressed by protein kinase C inhibitors. Given that asymmetric  $\text{Ca}^{2+}$  dysregulation precedes the cardiomyopathic stage, we speculate that abnormal  $\text{Ca}^{2+}$  handling in RV myocytes can be a trigger for gross structural changes observed at a later stage.

Joon-Chul Kim, PhD  
Marta Pérez-Hernández, PhD  
Francisco J. Alvarado, PhD  
Svetlana R. Maurya, PhD  
Jerome Montnach, PhD  
Yandong Yin, PhD  
Mingliang Zhang, PhD  
Xianming Lin, PhD  
Carolina Vasquez, PhD  
Adriana Heguy, PhD  
Feng-Xia Liang, PhD  
Sun-Hee Woo, PhD  
Gregory E. Morley, PhD  
Eli Rothenberg, PhD  
Alicia Lundby, PhD  
Hector H. Valdivia, MD, PhD  
Marina Cerrone, MD  
Mario Delmar, MD, PhD

**Key Words:** arrhythmogenic right ventricular cardiomyopathy ■ connexin43 ■ plakophilin 2 ■ right ventricle ■ sudden death

Sources of Funding, see page 1029

© 2019 American Heart Association, Inc.

<https://www.ahajournals.org/journal/circ>

## Clinical Perspective

### What Is New?

- This is the first demonstration that loss of Plakophilin-2 expression causes, as an early event and predominantly in the right ventricle (RV), a non-transcriptional, likely arrhythmogenic, Connexin43-dependent disruption of Ca<sup>2+</sup><sub>i</sub> homeostasis.
- The phenotype includes accumulation of Ca<sup>2+</sup> in 3 intracellular compartments: the junctional sarcoplasmic reticulum (SR), the cytoplasm, and the mitochondria. RV myocytes also show increased eagerness of ryanodine receptor 2 (RyR2) channels to release Ca<sup>2+</sup> from the SR.
- Intrinsic RyR2 properties are also modified; specifically, RV RyR2 channels have enhanced sensitivity to Ca<sup>2+</sup> and are selectively phosphorylated (likely by protein kinase C) at residue T2809, further contributing to the proarrhythmic state.

### What Are the Clinical Implications?

- Mutations in plakophilin-2 are the most common cause of gene-positive familial arrhythmogenic right ventricular cardiomyopathy.
- We postulate that disruption of Ca<sup>2+</sup><sub>i</sub> homeostasis in the RV is a major arrhythmia trigger in patients with arrhythmogenic right ventricular cardiomyopathy.
- Our data identified both the RyR2 channel and the Cx43 hemichannel as targets for antiarrhythmic therapy in the afflicted population.

**P**lakophilin-2 (PKP2) is classically defined as a protein of the desmosome, an intercellular adhesion structure. Recent studies demonstrated that in addition to cell-cell adhesion, PKP2 translates information initiated at the site of cell-cell contact into intracellular signals that maintain structural and electrical homeostasis.<sup>1–4</sup> Mutations in *PKP2* associate with most cases of gene-positive arrhythmogenic right ventricular cardiomyopathy (ARVC), a pleiotropic disease that can manifest as mainly electrical, structural, or both depending on stage progression.<sup>5</sup> As such, while ARVC is best recognized as a cardiomyopathy of right ventricular predominance, catecholaminergic sudden cardiac arrest is common during the subclinical, or “concealed”, phase of the disease.<sup>5–7</sup> The molecular/cellular mechanisms responsible for these arrhythmias remain unclear.

To study the role of cardiomyocyte PKP2 expression in cardiac function we used a cardiomyocyte-specific, tamoxifen (TAM)-activated, PKP2 knockout murine line (*PKP2* fl/fl,  $\alpha$ MyHC-Cre-ER(T2), dubbed PKP2cKO). We previously reported that adult PKP2cKO mice present, in a compressed time line, aspects of the history of human ARVC.<sup>3</sup> Following TAM injection these hearts progress from a normal state, to an arrhythmogenic

cardiomyopathy of right ventricular (RV) predominance and eventually biventricular dilated cardiomyopathy and end-stage failure. The time course of this process is reproducible, allowing us to study the molecular environment at a given phenotype stage.

The earliest functional event detectable in PKP2cKO mice is an increase in RV area (measured by echocardiography 14 days post-TAM injection) and a high propensity to Isoproterenol-induced lethal ventricular arrhythmias at day 16 post-TAM. These events occur in the setting of preserved left ventricular ejection fraction and in the absence of increased collagen abundance or other changes in ventricular wall morphology (ie, during a concealed stage preceding overt arrhythmogenic cardiomyopathy<sup>3,5,7</sup>). Thus, for this study we focused on mice 14 days post-TAM, so as to capture early molecular/cellular events that can act as nascent arrhythmia substrates. Knowing that PKP2 deficiency first leads to a structural phenotype of RV predominance<sup>3</sup> we separately studied myocytes from right versus left free ventricular walls. We focused on possible changes in intracellular Ca<sup>2+</sup> cycling, given previous evidence showing PKP2-mediated transcriptional regulation of intracellular Ca<sup>2+</sup> homeostasis in the cardiomyopathic stage.<sup>3</sup> Overall, we found that loss of PKP2 creates not only an RV-predominant cardiomyopathy but also an RV-predominant arrhythmogenic substrate that precedes the cardiomyopathy and that is, at least in part, dependent on Connexin 43 (Cx43) expression/function. We speculate that disrupted [Ca<sup>2+</sup>]<sub>i</sub> homeostasis in RV myocytes can be 1 of the triggers for gross structural changes in the RV at a later stage.

## METHODS

We used a commercially available C57BL/6 *CX43*<sup>flox</sup> mice line (Jackson Laboratory B6.129S7-Gja1<sup>tm1.1Dtg/J</sup>, stock number 008039; loxP sites flank exon 2 of *GJA1*; first reported by Liao et al<sup>8</sup> and extensively studied in various systems; see, eg, Hulsmans et al<sup>9</sup>), crossed with PKP2flox/flox/ $\alpha$ MHC-Cre-ER(T2) to obtain (CX43flox/flox)/(PKP2flox/flox)/Cre+, and CX43flox/wt/(PKP2flox/flox)/Cre+ mice. All procedures conformed to the Guide for Care and Use of Laboratory Animals of the National Institutes of Health and were approved by the NYU-IACUC committee. For cardiac-specific *PKP2* and/or *GJA1* deletion, mice were intraperitoneally injected 4 consecutive days with TAM (0.1 mg/g body weight). Cre-negative flox-positive, TAM-injected littermates were used as controls. Separate controls with TAM-injected, Cre-positive PKP2flox/wt showed no effects on life expectancy or left ventricular ejection fraction in a prolonged time window (Figure 1 in the online-only Data Supplement), consistent with previous observations.<sup>10</sup> Both genders were included and all animals were between 3 and 6 months-old. Further details in online-only Data Supplement.

Procedures used for RNAseq, cardiomyocyte dissociation, Ca<sup>2+</sup> imaging, Western blots, single-molecule localization microscopy, serial block-face scanning electron microscopy,

[<sup>3</sup>H]Ryanodine binding assays, mass spectrometry, echocardiography, patch clamp, and voltage-sensitive optical mapping followed those previously published and are detailed in the [online-only Data Supplement](#).

For evaluation of membrane permeability in whole hearts, 2 fluorescent dyes, Lucifer Yellow (LY) and Rhodamine Dextran, were used to quantify the entry of a small molecular weight dye into Langendorff-perfused hearts. Hearts were washed, fixed, epicardium was manually removed, free walls separated and placed epicardial face down for observation by fluorescence confocal microscopy. Imaging was performed at several randomly chosen sites in each tissue sample. Details in the [online-only Data Supplement](#).

## Statistical Analysis

Numerical results are given as means±SEM. Two-way repeated-measures ANOVA followed by Bonferroni post-hoc test was used for most data sets. In specific cases (noted in the respective figure legends), paired or unpaired Student *t* test, 1-way repeated-measures ANOVA-Bonferroni or Chi-square test was used. Analysis was done using OriginPro 8, Origin 2018b, SPSS 25 and SigmaPlot 13 packages. Differences were considered to be significant at *P*<0.05. Hierarchical analysis was performed as indicated in figure legends. Of note, this resource first detects adequacy of hierarchical analysis vis a vis other methods; analysis was performed accordingly for each data set.

## Data Availability

The data that support the findings of this study are presented in the article and online supplementary files. Additional information can be made available from the corresponding author upon reasonable request.

## RESULTS

### Ca<sup>2+</sup> Transients in Cardiomyocytes From PKP2cKO Hearts

We determined amplitude and time course of Ca<sup>2+</sup> transients of RV and LV myocytes from control and PKP2cKO hearts using conventional pacing protocols (e.g<sup>3</sup>). Figure 1A and 1B show time-space plots and time course of Ca<sup>2+</sup> transients, respectively, recorded by line-scanning confocal microscopy in cells loaded with Fluo-4 and field-stimulated at 1 Hz. Data from LV and RV (control and PKP2cKO) are shown to the left and right of the panels, respectively. Compiled data are shown in panels C-E. In this and subsequent figures, black and red bars represent data from control and PKP2cKO, respectively. The data show that transient amplitude was larger in PKP2cKO-RV myocytes when compared with either control, or PKP2cKO-LV myocytes (panel C). Loss of PKP2 also led to prolongation of Ca<sup>2+</sup> transient decay, which was statistically significant in RV myocytes (panel D). No difference was apparent in time-to-peak in either group (panel E). Of note, incidence of early

and delayed after-transients, and of spontaneous Ca<sup>2+</sup> waves, was significantly higher in PKP2cKO-RV myocytes when compared with PKP2cKO-LV myocytes or control (Figure II in the [online-only Data Supplement](#)).

Functional changes were accompanied by changes in protein abundance. Western blots showed reduced expression of PKP2 in both ventricles (Figure III in the [online-only Data Supplement](#)). In contrast, Ryanodine Receptor 2 (RyR2) abundance was higher in LV than RV of controls (Figure III in the [online-only Data Supplement](#)), and of PKP2cKO mice, rendering significant RV-LV asymmetry. Reduced SERCA2a was also observed in PKP2cKO-RV when compared with PKP2cKO-LV (Figure III in the [online-only Data Supplement](#)). Patch clamp experiments at fixed [Ca<sup>2+</sup>] detected no difference in peak NCX current density (Figure IV in the [online-only Data Supplement](#)).

### Increased Spontaneous Ca<sup>2+</sup> Release in PKP2cKO-RV Myocytes

Figure 1F shows confocal line-scan images of Ca<sup>2+</sup> sparks (arrows) from LV or RV intact cells of control or PKP2cKO mice 14 days post-TAM. Figure 1G through 1K show compiled results. Ca<sup>2+</sup> sparks frequency was similar for control myocytes regardless of provenance (RV or LV) and also similar to PKP2cKO-LV myocytes. However, the frequency of Ca<sup>2+</sup> sparks was significantly higher in PKP2cKO-RV myocytes (Figure 1G), though no difference in amplitude of events or full-width at half maximum was detected (Figure 1H and 1I). Ca<sup>2+</sup> sparks from PKP2cKO myocytes showed longer durations (full duration at half maximum; Figure 1J) and time-to-peak (Figure 1K). These results, together with those in Figure 1A through 1D, indicate that loss of PKP2 increases the propensity of RyR2 channels to release Ca<sup>2+</sup> preferentially in the RV. We therefore investigated whether this RyR2 eagerness associated with 1 or more of the following: a) a change in the transcriptional program of the cells (as it occurs during the cardiomyopathic stage<sup>3</sup>), b) functional changes intrinsic to the RyR2 protein, or c) an increase in the amount of Ca<sup>2+</sup> in the intracellular compartments.

### RNAseq RV Versus LV: No Major Transcriptional Differences

We examined the differential transcriptome (RV versus LV) of normal and PKP2cKO hearts (Complete datasets in [Tables I and II in the online-only Data Supplement](#)). Relative transcript abundance was determined from paired samples, by calculating the ratio RV/LV for each transcript in the same animal. Positive or negative Log<sub>2</sub>FC values therefore indicated over-representation of the transcript in RV or in LV, respectively.

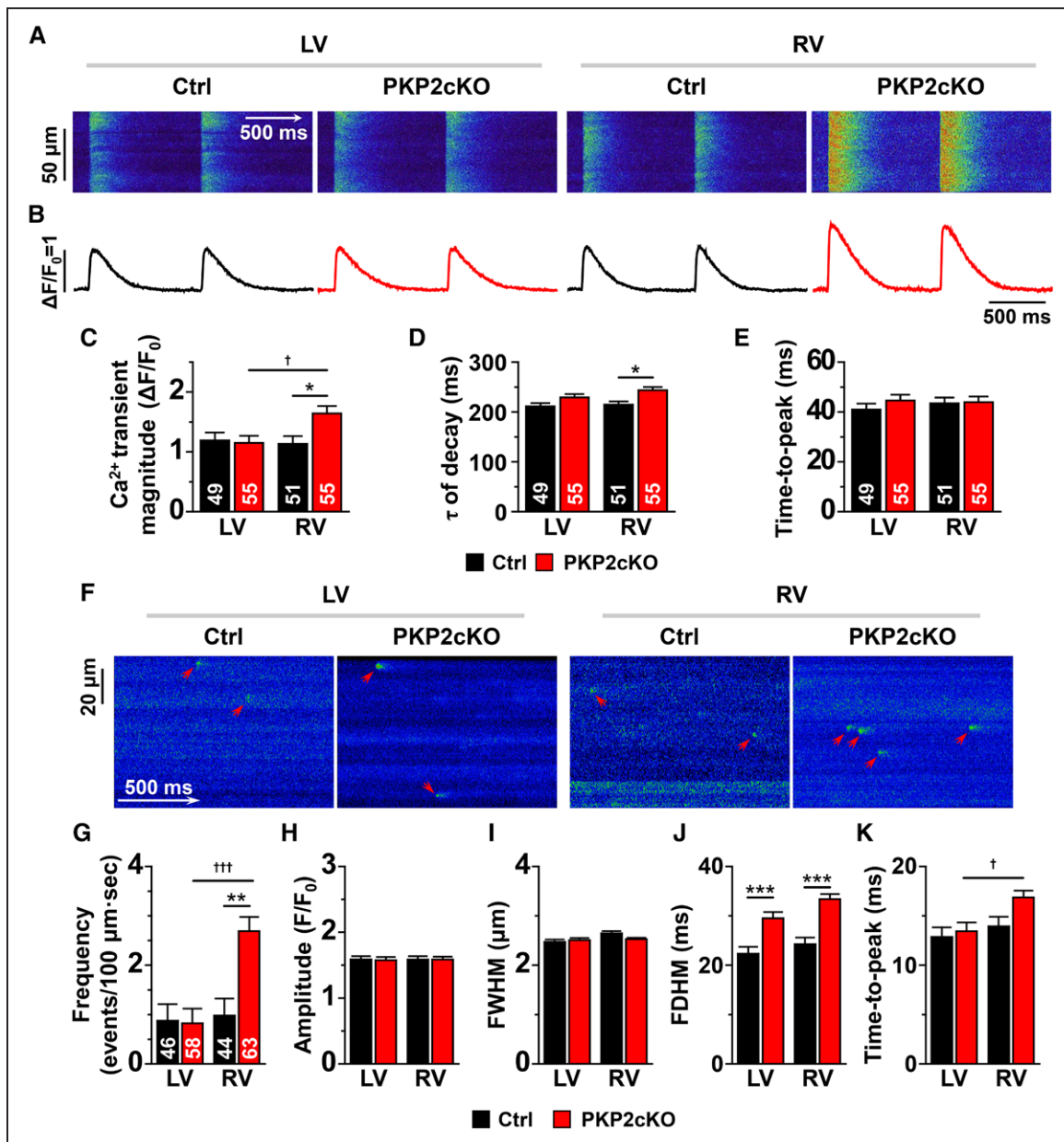


**Figure 1.** Ca<sup>2+</sup> transients and Ca<sup>2+</sup> sparks in right ventricle (RV) and left ventricle (LV) myocytes from control and plakophilin-2 conditional knockout (PKP2cKO) hearts.

Time-space plots (A) and time course of Ca<sup>2+</sup> transients (B) obtained by line-scans (1.43 ms/line) during field stimulation (1 Hz) of myocytes isolated from the LV and RV of control (Ctrl) and PKP2cKO mice. C through E, Compiled data for mean Ca<sup>2+</sup> transient magnitude (relative amplitude; ΔF/F<sub>0</sub>; C), time constant of Ca<sup>2+</sup> transient decay (ms; D), and time-to-peak (ms; E). Black and red bars depict data from Ctrl and PKP2cKO myocytes, respectively. F, Confocal line-scan images of Ca<sup>2+</sup> sparks (green; emphasized by red arrowheads) recorded from Ctrl and PKP2cKO myocytes isolated from either LV or RV. Cumulative data are shown in G through K. Black and red bars represent data obtained from Ctrl and PKP2cKO mice, respectively. G, Mean frequency of Ca<sup>2+</sup> sparks, reported as average number of events per second in a 100 μm line. H, Average peak amplitude (F/F<sub>0</sub>). I, Full-width at half maximum (FWHM; μm). J, Full duration at half maximum (FDHM; ms). K, Time-to-peak (ms). For all bar graphs: black, control; red, PKP2cKO. Number of cells studied is noted in the corresponding bars. For C through E: Statistical tests: Hierarchical test was first attempted. Output indicated whether to proceed via 2-way repeated-measures ANOVA-Bonferroni (details in Methods). Hierarchical test used for transient amplitude. Two-way repeated-measures ANOVA-Bonferroni for tau and time to peak. Total mice: 9 controls and 11 PKP2cKO. \**P*<0.05 vs control, †*P*<0.05 vs LV. For G through K: Numbers of sparks/cells/mice in control dataset: 618 sparks from 46 LV cells; 594 sparks from 44 RV cells; 6 mice. Numbers of sparks/cells/mice in PKP2cKO dataset: 675 sparks from 58 LV cells; 1842 sparks from 63 RV cells; 7 mice. Statistical test: Hierarchical analysis. See Methods for details. \*\**P*<0.01 vs control; \*\*\**P*<0.001 vs control; †*P*<0.05 vs LV; †††*P*<0.001 vs LV.

Volcano plots of differential transcriptomes (control and PKP2cKO mice) are presented in Figure V in the online-only Data Supplement. In controls, only 21 transcripts were differentially expressed with log<sub>2</sub>Fc values larger than ±1.0 and FDR values <0.01. Similar

results were obtained for the differential RV versus LV free wall transcriptome of PKP2cKO hearts, where only 9 transcripts were differentially expressed, and 4 of them were also differentially expressed in the controls. These results suggest that, as opposed to

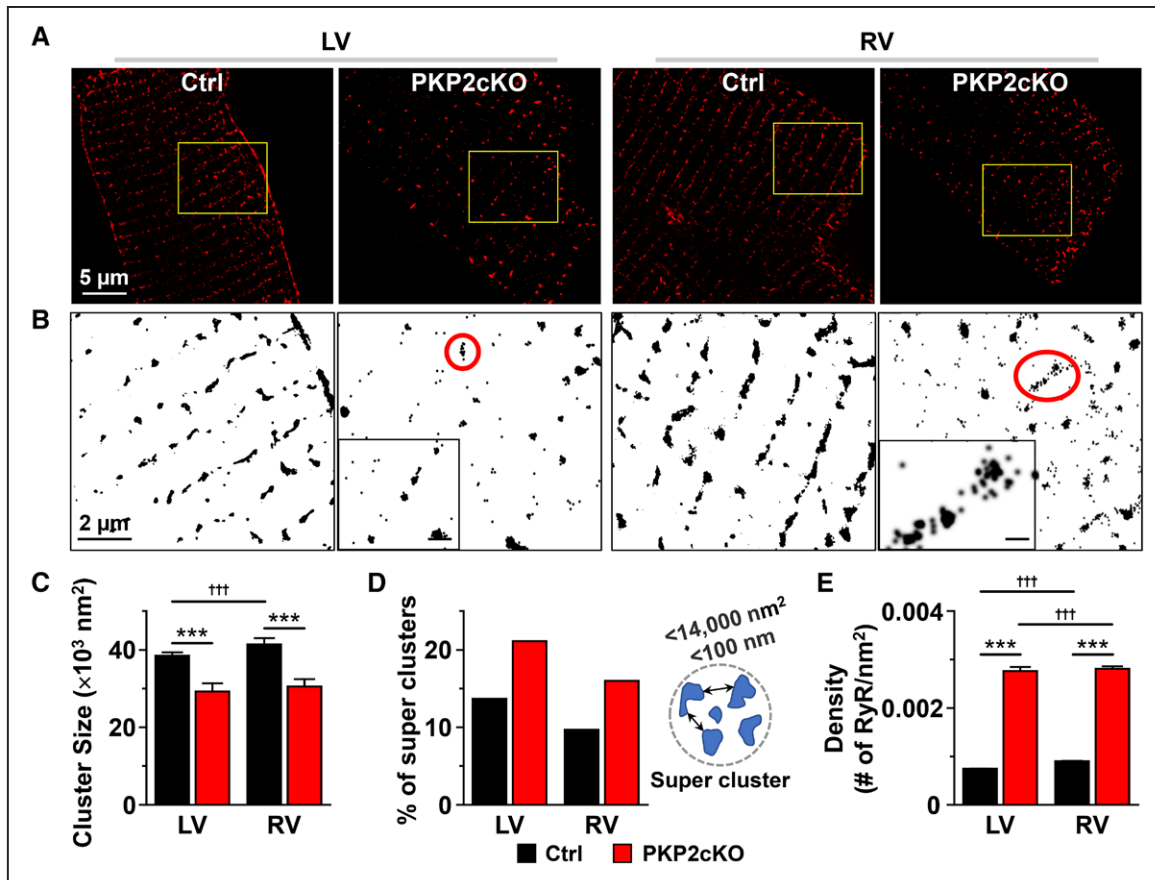


**Figure 2. Analysis of RyR2 clustering using single molecule-localization microscopy.**

**A**, Stochastic optical reconstruction microscopy (STORM)-acquired images of ryanodine receptor 2 (RyR2) in single myocytes dissociated from left ventricle (LV) or right ventricle (RV) of control (Ctrl) or plakophilin-2 conditional knockout (PKP2cKO) mice 14 days post-TAM. **B**, Yellow-boxed areas in **A** are shown in black and white for better visualization. Clusters within red circles in PKP2cKO are shown at larger magnification in the inset to illustrate the organization of small clusters in close proximity (scale bar in insets, 200 nm). **C**, Average size of RyR2 clusters in control and PKP2cKO myocytes. Control: n=24158 clusters from 11 LV cells; 14906 clusters from 8 RV cells. PKP2cKO: n=27365 clusters from 19 LV cells; 31852 clusters from 18 RV cells. **D**, Bar graph shows the proportion of super-clusters in control or PKP2cKO myocytes. LV control: 3280 super-clusters/23946 total clusters; LV PKP2cKO: 1581 super-clusters/7481 total clusters; RV control: 1435 super-clusters/14815 total clusters; RV PKP2cKO: 1534 super-clusters/9586 total clusters. Criteria used for defining super-clusters is diagrammed at the right of the panel. **E**, RyR2 molecular density, estimated as the number of RyR2 molecules (calculated by Density-Based Spatial Clustering of Applications with Noise; DBSCAN) per unit of cluster area (see also Methods). Number of clusters analyzed (including clusters with at least 10 RyRs): 32738 LV and 16595 RV clusters from control; 1666 LV and 4396 RV clusters from PKP2cKO. Statistical significance by 2-way repeated-measures ANOVA-Bonferroni test: \*\*\* $P < 0.001$  vs control; ††† $P < 0.001$  vs LV.

what occurs at the cardiomyopathic stage,<sup>3</sup> our data cannot be explained by PKP2-dependent changes in transcript abundance of molecules directly involved in regulation of Ca<sup>2+</sup> homeostasis.

## Structural and Functional Properties of RyR2 in PKP2cKO Myocytes

We examined 3 aspects of RyR2: its nanostructural organization into clusters, sensitivity to Ca<sup>2+</sup>, and phosphorylation state.

### RyR2 Super-Clusters in PKP2cKO Myocytes

Recent studies show that when 2 small RyR2 clusters are at a distance of  $\leq 100$  nm from each other, the probability for propagating Ca<sup>2+</sup> release is increased ("super-clusters"<sup>11–13</sup>). Data also show that a heterogeneous population of clusters (co-existence of

super-clusters and large single clusters) can lead to increased susceptibility to calcium waves.<sup>14</sup> Figure 2A shows single-molecule localization microscopy images of clusters of RyR2 from control or PKP2cKO adult ventricular myocytes 14 days post-TAM. In Figure 2B, areas in yellow boxes are enlarged and displayed in black and white to enhance contrast. All clusters were analyzed for size and proximity.<sup>15</sup> RyR2 clusters were, on average, significantly smaller in PKP2cKO cells (Figure 2C). The subpopulation of clusters occupying an area  $\leq 14,000$  nm<sup>2</sup> (such as those in insets of Figure 2B) was subsequently analyzed to identify the fraction of clusters whose edges were within 100 nm from each other (super-clusters; see diagram in Figure 2D). Cumulative data (Figure 2D) show that the proportion of super-clusters was higher in PKP2cKO and that they co-existed with large clusters, forming a heterogeneous population likely to provide a structural substrate for

enhanced Ca<sup>2+</sup> release.<sup>14</sup> Importantly, the frequency of super-clusters was similar in myocytes from RV versus LV of PKP2cKO mice. We then calculated the number of RyR2 units and their density utilizing Density-Based Spatial Clustering of Applications with Noise (see the [online-only Data Supplement](#)). The median number of RyR2 units per cluster (between 30 and 58 RyR2 units; [Figures VI and VII in the online-only Data Supplement](#)) was within the range of what has been previously reported.<sup>11–13</sup> However, the density of RyR2 units within a cluster (number of RyR2 units per nm<sup>2</sup>) was significantly larger in PKP2cKO cells when compared with control (Figure 2E), likely facilitating cross-activation of Ca<sup>2+</sup> induced Ca<sup>2+</sup> release. Yet, the absence of right-left asymmetry suggests that this difference is not, per se, a mechanism for preferential increased Ca<sup>2+</sup> release in RV myocytes. As a next step, we examined the Ca<sup>2+</sup> sensitivity and phosphorylation state of RyR2 channel proteins.

### **Reduced Expression and Enhanced Ca<sup>2+</sup> Sensitivity of RyR2 in PKP2cKO-RV Myocytes**

[<sup>3</sup>H]Ryanodine binding assays were performed from right and left ventricular tissue, harvested 14 days post-TAM, to determine Ca<sup>2+</sup> sensitivity of RyR2 channels in PKP2cKO hearts versus controls. The plots in Figure 3A and 3B and the bar graph in Figure 3C show that, while samples collected from the PKP2cKO-LV showed a similar Ca<sup>2+</sup> response as controls, samples from the RV of PKP2cKO mice showed a lower B<sub>max</sub>, consistent with lower RyR2 expression ([Figure VIII in the online-only Data Supplement](#)). Normalization of [<sup>3</sup>H]ryanodine binding to levels observed at the highest Ca<sup>2+</sup> concentration (10 μmol/L) revealed no difference between PKP2cKO-LV and control samples, but a left-shift (enhanced Ca<sup>2+</sup> sensitivity; reduced EC<sub>50</sub>) for PKP2cKO-RV hearts (Figure 3D through 3F).

### **Differential Phosphorylation State of RyR2: Phosphorylation of T2809 in the RV**

In addition to Ca<sup>2+</sup> sensitivity, sarcoplasmic reticulum (SR) Ca<sup>2+</sup> release can be modulated by RyR2 phosphorylation.<sup>16–18</sup> Accordingly, we evaluated the phosphorylation state of RyR2 in RV and LV of 4 PKP2cKO mice 14 days post-TAM using high-resolution mass spectrometry<sup>19</sup> (see the [online-only Data Supplement](#)). Our measurements covered 13 phosphorylation sites on RyR2, 11 of which were class 1 sites with high confidence in phosphorylation site localization (Figure 4A). Figure 4B presents a summary of intensity measurements of all RyR2 phosphopeptides across samples. Notice that amino acids S2807 and S2813, previously characterized as preferential substrates for PKA and CAMKII respectively (and annotated as “S2808” and “S2814” in the old nomenclature), are detected as phosphorylated in all samples, irrespective of provenance. However, there was a clear distinction between phosphorylation

states of residue T2809. All 4 PKP2cKO-RV samples showed high levels of T2809 phosphorylation, whereas phosphorylation on this residue was not detected in samples from PKP2cKO-LV. Figure 4C shows a tandem mass spectrometry spectrum of T2809 phosphorylation measured in a PKP2cKO-RV sample underscoring the certainty in site localization to this residue. T2809, not previously characterized as substrate for kinase regulation of RyR2 and yet located in the same phosphorylation “hotspot” known to regulate RyR2 gating<sup>20</sup> is highly conserved across species. Samples from over 120 000 individuals deposited in gnomAD show no variance in T2809, suggesting biological relevance. According to NetPhos3.1 ([www.cbs.dtu.dk/services/NetPhos/](http://www.cbs.dtu.dk/services/NetPhos/)), the probability of T2809 to be a protein kinase C (PKC) substrate is estimated at 0.721 in the human sequence and 0.671 in the case of mouse ([Figure IX in the online-only Data Supplement](#)).<sup>21,22</sup> The bar graph in Figure 4D summarizes the results and shows that T2809 phosphorylation was also absent in 4 control hearts. Interestingly, S2810, another phosphorylation site not yet fully characterized and located within the same hotspot, was phosphorylated exclusively in PKP2cKO samples, though to a similar level in RV and LV (Figure 4D).

## **Intracellular Ca<sup>2+</sup> Content**

### **Increased SR Load in PKP2cKO RV Myocytes**

In addition to properties intrinsic to RyR2, we examined whether enhanced Ca<sup>2+</sup> sparks coincided with differences in abundance of stored Ca<sup>2+</sup> in the intracellular space. The SR Ca<sup>2+</sup> load of intact (non-permeabilized) myocytes was estimated from the amplitude of caffeine-induced Ca<sup>2+</sup> transients, using a ratiometric dye method.<sup>23,24</sup> As shown in Figure 5A and 5B, SR Ca<sup>2+</sup> content of PKP2cKO-RV myocytes was higher than in PKP2cKO-LV or in myocytes from controls (Figure 5B and 5C). Similar results were obtained from permeabilized myocytes using a method previously implemented in our laboratory<sup>3</sup> ([Figure X in the online-only Data Supplement](#)).

### **Increased [Ca<sup>2+</sup>] in the Cytoplasmic and Mitochondrial Compartments**

The SR was not the only intracellular compartment with increased Ca<sup>2+</sup> load. Indeed, as shown in Figure 5D and 5E, cytoplasmic resting Ca<sup>2+</sup> content was higher in PKP2cKO myocytes (see also [Figure X in the online-only Data Supplement](#)). Furthermore, using a Ca<sup>2+</sup> indicator (Rhod-2) that enters the mitochondrial space in a temperature-dependent manner (see also [Figure XI in the online-only Data Supplement](#)),<sup>25</sup> we unveiled a dynamic Ca<sup>2+</sup> accumulation in mitochondria of isolated PKP2cKO-RV myocytes after a brief period of pacing (1 minute at 3 Hz; Figure 5F and 5G). Altogether, the

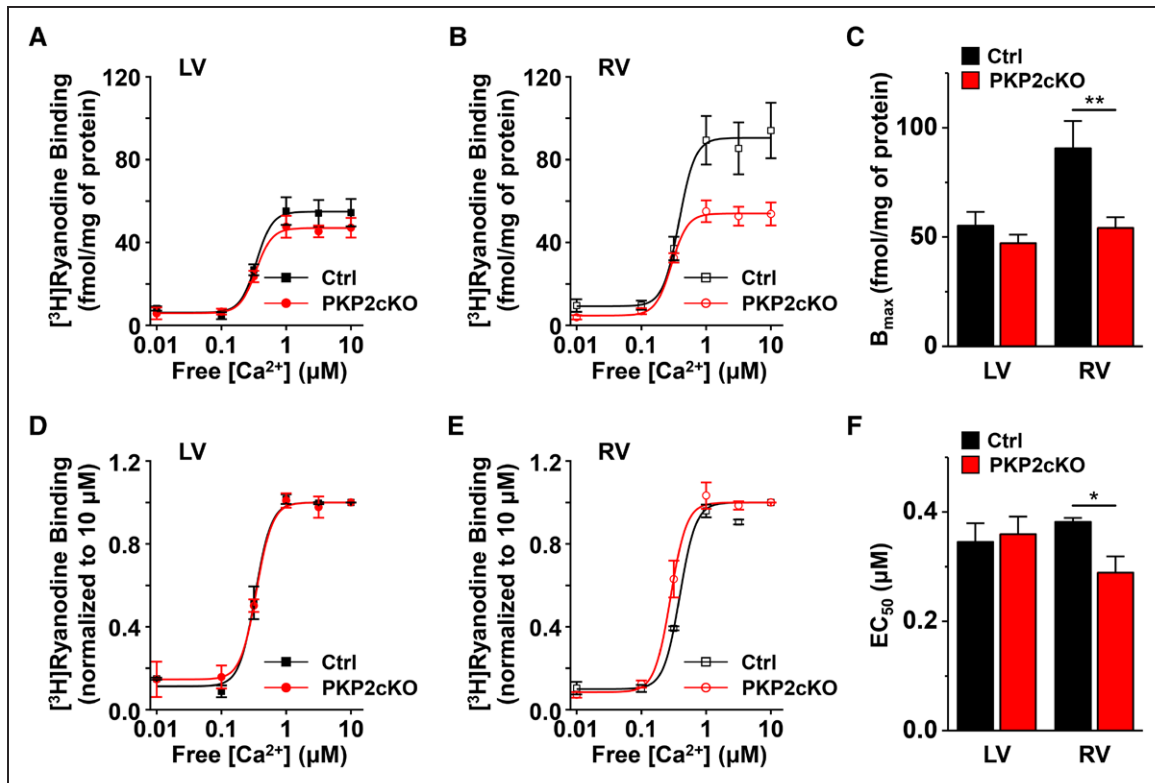


**Figure 3.** [<sup>3</sup>H]Ryanodine binding in homogenates from control or PKP2cKO hearts.

**A**, [<sup>3</sup>H]Ryanodine binding as a function of free [Ca<sup>2+</sup>] in samples obtained from the left ventricle (LV) of either control (Ctrl) or plakophilin-2 conditional knockout (PKP2cKO) hearts 14 days post-TAM. **B**, Same as **A** but for samples obtained from the right ventricle (RV). Cumulative data for binding maximum (B<sub>max</sub>) is shown in **C**. Data normalized for the binding observed at 10 μmol/L free [Ca<sup>2+</sup>] for LV and RV are shown in **D** and **E**, respectively. This correction allowed us to observe a shift in the concentration of free [Ca<sup>2+</sup>] that produces 50% of maximal [<sup>3</sup>H]Ryanodine binding (EC<sub>50</sub>) in the RV tissue of PKP2cKO hearts (**F**). n=4 hearts for each group. \*P<0.05 vs control, \*\*P<0.01 vs control. Two-way repeated-measures ANOVA–Bonferroni test.

results reveal increased [Ca<sup>2+</sup>] in all 3 major compartments (SR, cytoplasmic, and mitochondrial) in PKP2cKO-RV myocytes when compared with PKP2cKO-LV or control myocytes.

### Spark Frequency at Comparable SR Load: Effect of PKC Inhibition

The observations above raised the question of whether increased spark frequency in PKP2cKO-RV myocytes was consequent to increased SR load, enhanced RyR2 release of Ca<sup>2+</sup>, or both. We therefore analyzed spark frequency at comparable levels of SR load using a procedure similar to that of Kim et al.<sup>26</sup> Control experiments showed that reducing [Ca<sup>2+</sup>]<sub>o</sub> to 0.6 mmol/L in PKP2cKO-RV myocytes yielded a comparable SR load to that obtained in PKP2cKO-LV myocytes at 1.8 mmol/L [Ca<sup>2+</sup>]<sub>o</sub> (see [Figure XII in the online-only Data Supplement](#)). Under those circumstances, spark frequency decreased, but remained higher than that observed in either control myocytes or in PKP2cKO-LV cells (Figure 6; blue bars). Further reduction of spark frequency was obtained when GF 109203X or Calphostin C, both inhibitors of PKC activity,<sup>26</sup> were added to the external solution (blue bars with a + sign in Figure 6E). These results indicate that both increased SR load and enhanced RyR2 Ca<sup>2+</sup> release contribute to heightened

abundance of calcium sparks in PKP2cKO-RV myocytes, and that the latter is susceptible to inhibition by PKC antagonists.

### Increased Membrane Permeability in PKP2cKO-RV Myocytes: Role of Cx43

The results above led to the question of the source of excess intracellular Ca<sup>2+</sup>. As one possibility, we examined whether increased membrane permeability would be a factor, and whether the permeable conduit would be dependent on Cx43 expression. Considering that Cx43 internalizes after dissociation,<sup>27</sup> we devised a protocol for analysis of LY (mw 457) transfer in Langendorff-perfused whole heart preparations (see Methods). Figure 7A shows fluorescence confocal images of a control (left) and a PKP2cKO mouse heart 14 days post-TAM (middle). Images were collected from LV (top) and RV (bottom). Of note, Rhodamine Dextran (mw ~10,000 Da) was also loaded and was not found in the intracellular space, confirming that LY did not enter cells through damaged sarcolemma (see [Figure XIII in the online-only Data Supplement](#)). A quantitative analysis is shown in Figure 7B (black and red bars). Notice the increased fluorescence apparent in PKP2cKO

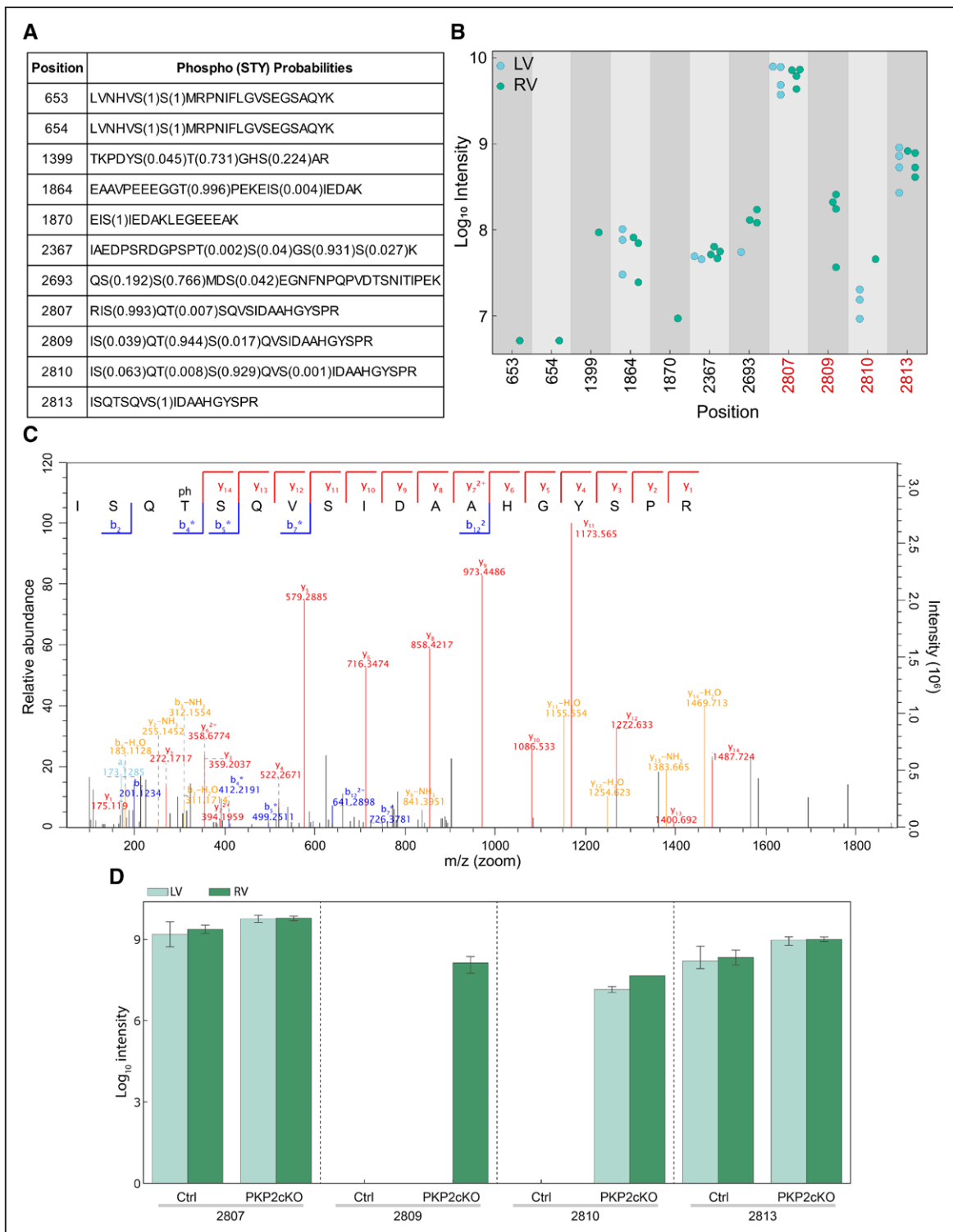


**Figure 4.** Mass spectrometry–based investigation of ryanodine receptor 2 (RyR2) phosphorylation state in left ventricle (LV) vs right ventricle (RV) of PKP2cKO hearts.

**A**, Summary of the 11 class-1 phosphopeptides identified. The first column indicates the position of the phosphorylated amino acid in the RyR2 sequence, and the second column indicates the amino acid sequence of the peptide in which the phosphorylation site was measured. The numbers in brackets indicate the probability with which the localization of the phosphorylation site has been assigned to that particular residue (assignment of phosphorylation site localization depends on fragmentation pattern). **B**, Mass spectrometry–based intensity measurements of phosphopeptides covering the 11 phosphorylation sites. Intensities of all measured phosphopeptides are displayed. Measurements from RV samples are depicted in green, and measurements from LV samples are indicated in blue. The phosphorylation hot spot of RyR2 is highlighted in red. Phosphorylation of site 2809 was exclusively identified in RV samples. **C**, Measured peptide covering T2809 is shown along with the detected fragment ions indicated. The fragment ions are highlighted in the tandem mass spectrometry (MS/MS) spectrum. The peptide contained 1 phosphate group, and because of the fragmentation pattern the phosphorylation site could be localized to threonine 2809. **D**, Data summary. Mass spectrometry–based intensity measurements of phosphopeptides covering the 4 phosphorylation sites in the hot spot region of RyR2 from tissue samples control (Ctrl) and plakophilin-2 conditional knockout (PKP2cKO) mice. Measurements from LV and RV samples depicted in light and dark green, respectively.  $n=3$  for control samples and  $n=4$  for PKP2cKO samples.

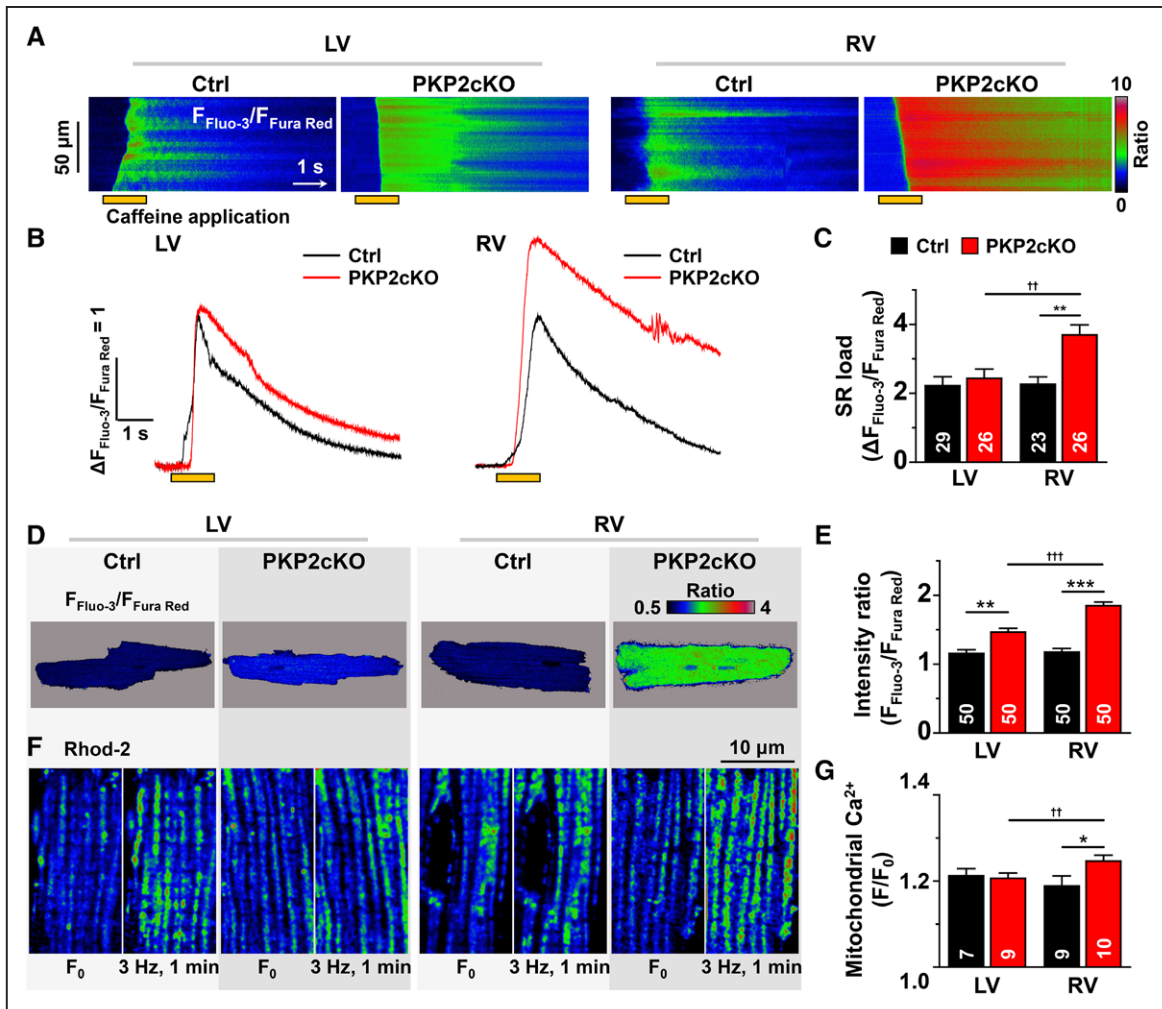


**Figure 5.** Ca<sup>2+</sup> content in the intracellular compartments.

**A**, Confocal line-scan images (1.43 ms/line) recorded from nonpermeabilized myocytes isolated from the free walls of the left ventricle (LV) or the right ventricle (RV) of either control (Ctrl) or plakophilin-2 conditional knockout (PKP2cKO) mice 14 days post-tamoxifen (post-TAM). In this and other panels, the pulse of caffeine (10 mmol/L) is indicated by the orange bar at the bottom of the image. Intracellular calcium changes were detected by a ratiometric method ( $F_{\text{Fluo-3}}/F_{\text{Fura Red}}$ ; see also Methods). **B**, Time course and amplitude of the change in fluorescence during and immediately after the caffeine pulse. Notice the larger amplitude of the transient recorded from PKP2cKO RV myocytes. Cumulative data are shown in **C**. Number of experiments noted in the bar graphs. Cells originated from 5 different mice in each group (Ctrl or PKP2cKO). Statistical test: 2-way repeated-measures ANOVA-Bonferroni. Control: n=29 LV cells, 23 RV cells. PKP2cKO: n=26 LV cells, 26 RV cells. \*\* $P<0.01$  vs control, †† $P<0.01$  vs LV. **D**, Pseudo-colored confocal 2D images of the ratio of emission intensities ( $F_{\text{Fluo-3}}/F_{\text{Fura Red}}$ ; see also Methods). The average of the calculated intensity ratios is shown in **E**. Statistical test: Hierarchical analysis. Control: n=50 LV cells, 50 RV cells from 5 mice. PKP2cKO n=50 LV cells, 50 RV cells from 5 mice. \*\* $P<0.01$  vs control, \*\*\* $P<0.001$  vs control, ††† $P<0.001$  vs LV. **F**, Confocal 2-D images of cardiomyocytes loaded with 2  $\mu\text{mol/L}$  Rhod 2-AM at low temperature (4°C) and then incubated at 37°C for 4 hours (see also Methods). For each group, 2 images from the same cell are shown: at rest ( $F_0$ ; left), and after 1 minute stimulation at 3 Hz (right). Notice the increased number of fluorescence emission units (mitochondria) after stimulation, particularly in the cell from the PKP2cKO RV. **G**, Average of the ratio of Rhod-2 fluorescence intensities acquired before ( $F_0$ ) and after (F) the period of pacing. Control (Ctrl): n=7 LV cells, 9 RV cells from 2 mice. PKP2cKO: n=9 LV cells, 10 RV cells from 2 mice. Statistical test: 2-way repeated-measures ANOVA-Bonferroni. \* $P<0.05$  vs control, †† $P<0.01$  vs LV.

hearts, more prominently in the RV (black versus red bars in Figure 7B).

Neither the abundance nor the subcellular localization of Cx43 were affected by loss of PKP2 expression at 14 days post-TAM (Figure XIV in the online-only Data Supplement). To define whether increased fluorescence was dependent on Cx43 function, we crossed PKP2cKO mice with a commercially available Cx43 fl/fl line<sup>8</sup> to obtain, in response to TAM, a double PKP2-Cx43 knockout (referred to as PKP2-Cx43cKO). The mice developed normally and heart function prior to TAM was not different from control. As previously reported, life expectancy

in Cx43-KO animals is limited, given their high likelihood of arrhythmic death.<sup>28–30</sup> Two out of 4 TAM-injected animals survived to day 14 post-TAM. As shown in Figure 7A (right column) and Figure 7B (blue bars), loss of Cx43 expression blunted the excess LY signal captured from either LV or RV. Interestingly, the increased membrane permeability was observed for both RV and LV PKP2cKO samples at a later time (21 days post-TAM; Figure XV in the online-only Data Supplement) and in both cases, reduced Cx43 (PKP2cKO and Cx43 heterozygous; PKP2cKO/Cx43<sup>+/−</sup>) was sufficient to limit the increased membrane permeability to LY (green versus

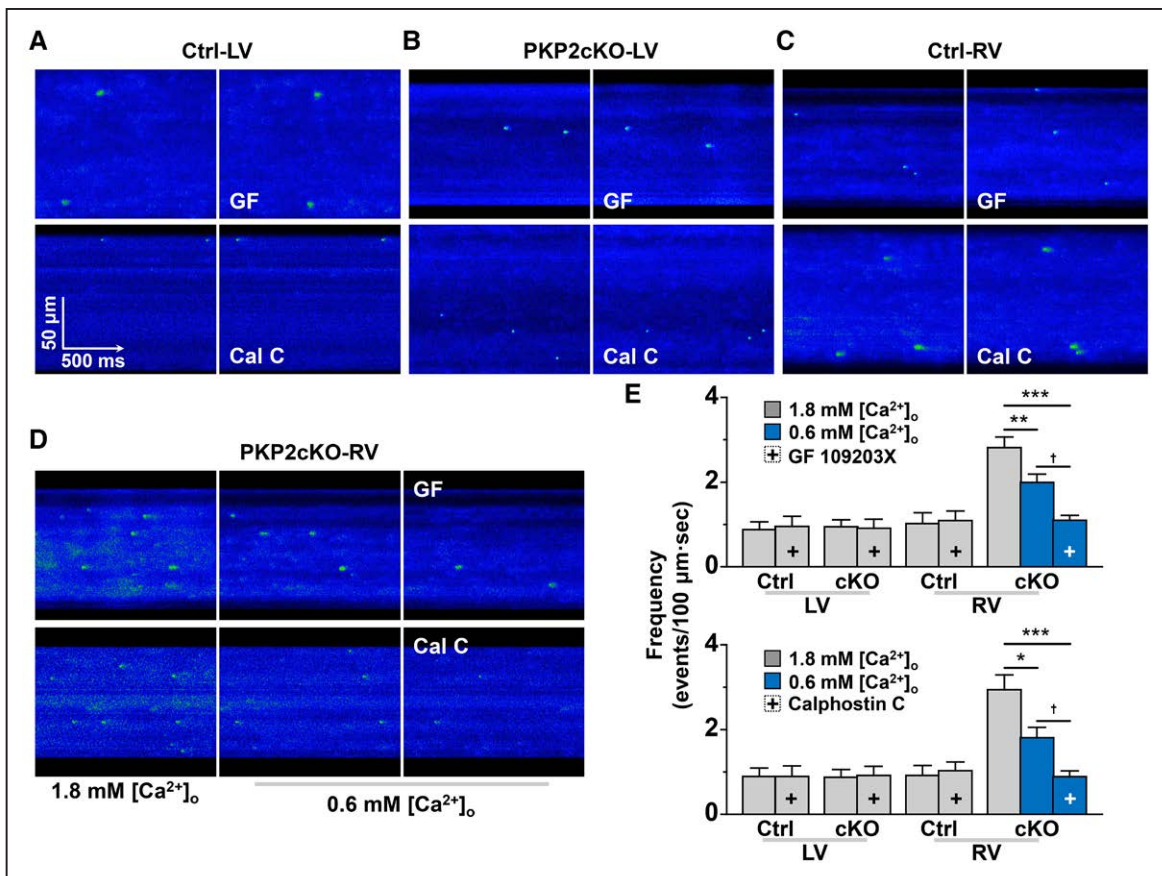


**Figure 6. Spark frequency at equal sarcoplasmic reticulum (SR) load and effect of protein kinase C (PKC) inhibition.**

**A** through **D**, Confocal line-scan images of  $\text{Ca}^{2+}$  sparks (green) in Control (Ctrl; **A** and **C**) or plakophilin-2 conditional knockout (PKP2cKO) samples (**B** and **D**) obtained from the left ventricle (LV; **A** and **B**) or the right ventricle (RV; **C** and **D**). **D** shows sparks obtained when cells were maintained in either 1.8 mmol/L  $[\text{Ca}^{2+}]_o$  (**left**) or in 0.6 mmol/L  $[\text{Ca}^{2+}]_o$  (**middle** and **right**). In **A** through **D**, **right-most panel** corresponds to data obtained in the presence of PKC inhibitors bisindolylmaleimide I (GF 109203X; labeled GF; **top**) or Calphostin C (labeled Cal C; **bottom**). **E**, Spark (spontaneous calcium release [SCR]) events measured under the various conditions. + indicates in the presence of the PKC inhibitor (GF 109203X, **top**; Calphostin C, **bottom**). Blue bars, data obtained at 0.6 mmol/L  $[\text{Ca}^{2+}]_o$ . All experiments were performed in sequence on the same cell: recordings at  $[\text{Ca}^{2+}]_o$  1.8 mmol/L, then switched to 0.6 mmol/L  $[\text{Ca}^{2+}]_o$  (for PKP2cKO RV) and then addition of PKC inhibitor. Each group was treated separately and only 1 variable (SCR frequency) was measured. cKO means plakophilin-2 conditional knockout. Paired sample *t* test for Ctrl LV, Ctrl RV, PKP2cKO-LV (same cell compared before and after treatment). One-way repeated-measures ANOVA-Bonferroni for PKP2cKO-RV (same cell compared at  $[\text{Ca}^{2+}]_o$  1.8 mmol/L, then at 0.6 mmol/L  $[\text{Ca}^{2+}]_o$  and then treatment). For experiments with GF 109203X: Control n=8 LV cells, 9 RV cells from 3 mice. PKP2cKO n=6 LV cells, 15 RV cells from 3 mice. \*\**P*<0.01, \*\*\**P*<0.001 vs 1.8 mmol/L  $[\text{Ca}^{2+}]_o$ ; †*P*<0.05 vs 0.6 mmol/L  $[\text{Ca}^{2+}]_o$ . For experiments with Calphostin C: Control n=9 LV cells, 7 RV cells from 3 mice. PKP2cKO n=11 LV cells, 13 RV cells from 3 mice. \**P*<0.05, \*\*\**P*<0.001 vs 1.8 mmol/L  $[\text{Ca}^{2+}]_o$ ; †*P*<0.05 vs 0.6 mmol/L  $[\text{Ca}^{2+}]_o$ .

red bars in Figure XV in the online-only Data Supplement). These results suggest that in the PKP2cKO there is a Cx43-dependent mechanism in place that allows for small molecules to enter the cytoplasmic space.

### Reduced Cx43 Normalized Diastolic $[\text{Ca}^{2+}]_i$ and Spark Frequency in PKP2cKO Hearts

Based on the results in Figure 7A and 7B we tested whether elevated levels of diastolic  $\text{Ca}^{2+}$  and/or increased  $\text{Ca}^{2+}$  spark frequency in PKP2cKO-RV myocytes could be prevented by reducing Cx43 abundance. As shown in Figure 7C, cells obtained from PKP2cKO mice also heterozygous-null for cardiomyocyte Cx43 (PKP2cKO/Cx43<sup>+/-</sup>) showed a level of  $[\text{Ca}^{2+}]_i$  that was not different from control. Spark frequency (at 1.8 mmol/L  $[\text{Ca}]_o$ ) was significantly reduced when compared with

that obtained from PKP2cKO-RV cells, though remained higher than what was observed in control RV myocytes (Figure 7D).

To further ascertain the role of Cx43, we examined SR load, spark frequency and  $\text{Ca}^{2+}$  transient amplitude in PKP2cKO myocytes exposed to the Cx43 hemichannel inhibitor TAT-Gap 19 (see also Figure XVI in the online-only Data Supplement).<sup>31,32</sup> As shown in Figure 8, this manipulation blunted the effect of PKP2 knockdown, reducing all parameters to levels that, for SR load, diastolic  $[\text{Ca}^{2+}]_i$ , and transient amplitude, were not significantly different from those observed in PKP2cKO-LV or control myocytes. As in the case of the PKP2cKO/Cx43<sup>+/-</sup> cells, spark frequency remained slightly higher in PKP2cKO-RV after GAP19, perhaps reflecting a direct effect of PKP2 knockdown on RyR2 function independent from increased Cx43-dependent calcium load.

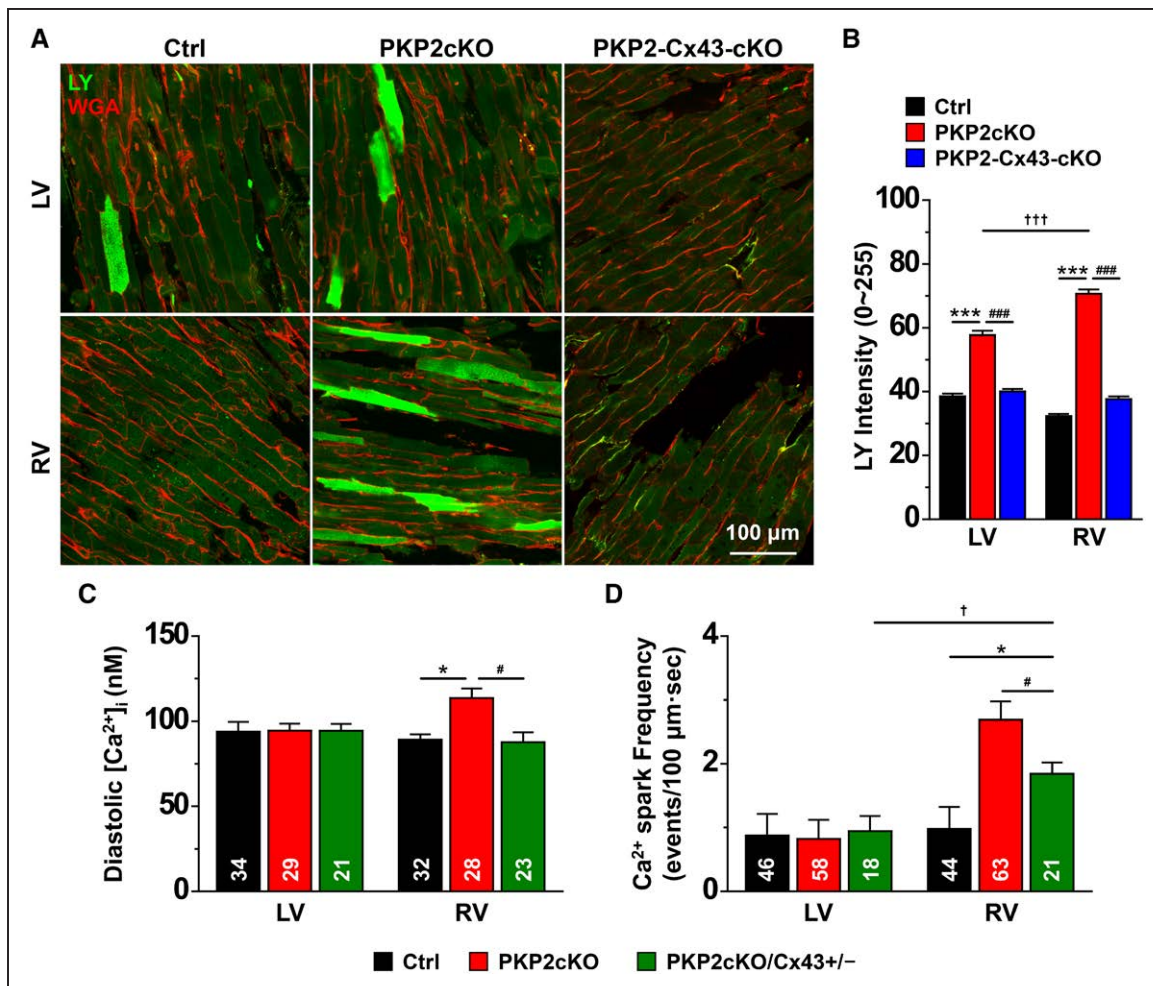


**Figure 7. Membrane permeability to Lucifer Yellow and Connexin 43 (Cx43) expression.**

**A**, Confocal images collected from the epicardial phase of either the free walls of the left ventricle (LV) or the right ventricle (RV) of hearts harvested from control (Ctrl), plakophilin-2 conditional knockout (PKP2cKO) mice 14 days post-tamoxifen (post-TAM) or a double knockout of PKP2 and Cx43, also at 14 days post-TAM (PKP2-Cx43-cKO). Images were obtained after a 30-min perfusion with 1 mg/mL Lucifer Yellow (LY; molecular weight 457; green), 1 mg/mL Rhodamine Dextran (molecular weight ~10 000), and 0.04 mg/mL Wheat Germ Agglutinin (WGA; red) in 10 nmol/L free  $[Ca^{2+}]_i$  solution (see Methods for further details). Image fields were chosen at random, and the intensity of the LY fluorescence (in a scale 0–225) was measured within regions of interest (ROIs) that excluded areas void of cells. **B**, Average LY intensity measured from cells in the following groups: Control (Ctrl; black bars; n=512 LV cells, 774 RV cells from 3 mice), PKP2cKO (red bars; n=763 LV cells, 812 RV cells from 3 mice) and PKP2-Cx43-cKO (blue bars; n=617 LV cells, 729 RV cells from 2 mice). Statistical test: 2-way repeated-measures ANOVA-Bonferroni \*\*\* $P$ <0.001 vs control; ††† $P$ <0.001 vs LV; ### $P$ <0.001 vs PKP2cKO. **C**, Mean of the calculated values of  $[Ca^{2+}]_i$  after calibration of intensity ratios (see Methods for details). Control: n=34 LV cells, 32 RV cells from 4 mice. PKP2cKO n=29 LV cells, 28 RV cells from 4 mice. PKP2cKO/Cx43<sup>+/-</sup> refers to a PKP2cKO mice also heterozygous-null for Cx43 in cardiomyocytes (see also Methods). n=21 LV cells, 23 RV cells from 3 mice. Statistical test: Hierarchical analysis. \* $P$ <0.05 vs control; # $P$ <0.05 vs PKP2cKO. **D**,  $Ca^{2+}$  spark frequency is significantly dampened by reduced Cx43 expression (green bar). Note that data for RV and LV Ctrl and PKP2cKO are reproduced from previous figures and presented here for comparison against PKP2cKO/Cx43<sup>+/-</sup>. Hierarchical analysis: PKP2cKO/Cx43<sup>+/-</sup>: n=18 LV cells, 21 RV cells from 3 mice. \* $P$ <0.05 vs control; † $P$ <0.05 vs LV; # $P$ <0.05 vs PKP2cKO.

## Reduced Cx43 Mitigated the Increase in RV Area in PKP2cKO Hearts

The earliest functional event reported for PKP2cKO hearts was an increase in RV area at 14 days post-TAM.<sup>3</sup> As shown by the green bars in [Figure XVII in the online-only Data Supplement](#), a reduction in Cx43 gene dose mitigated the increase in RV area, which was significantly smaller in PKP2cKO/Cx43<sup>+/-</sup> when compared with PKP2cKO mice at 14 days post-TAM. This result further supports the notion of a role for Cx43 in the early stage pathophysiology that results from PKP2 loss of expression.

## PKP2cKO and Cellular/Subcellular Structure at 14 Days Post-TAM

We evaluated whether the events described above were associated with structural changes at the cellular/subcellular level. Measurements of cell size (length, width and area), membrane capacitance (as a surrogate for sarcolemmal surface area), and sarcomere length were not different between the 4 groups (Control and PKP2cKO; RV and LV; [Figure XVIII in the online-only Data Supplement](#)). Interestingly, single-molecule localization microscopy of phospho-PKC localization (T368-641) at the cell end showed reduced cluster size and a tenden-

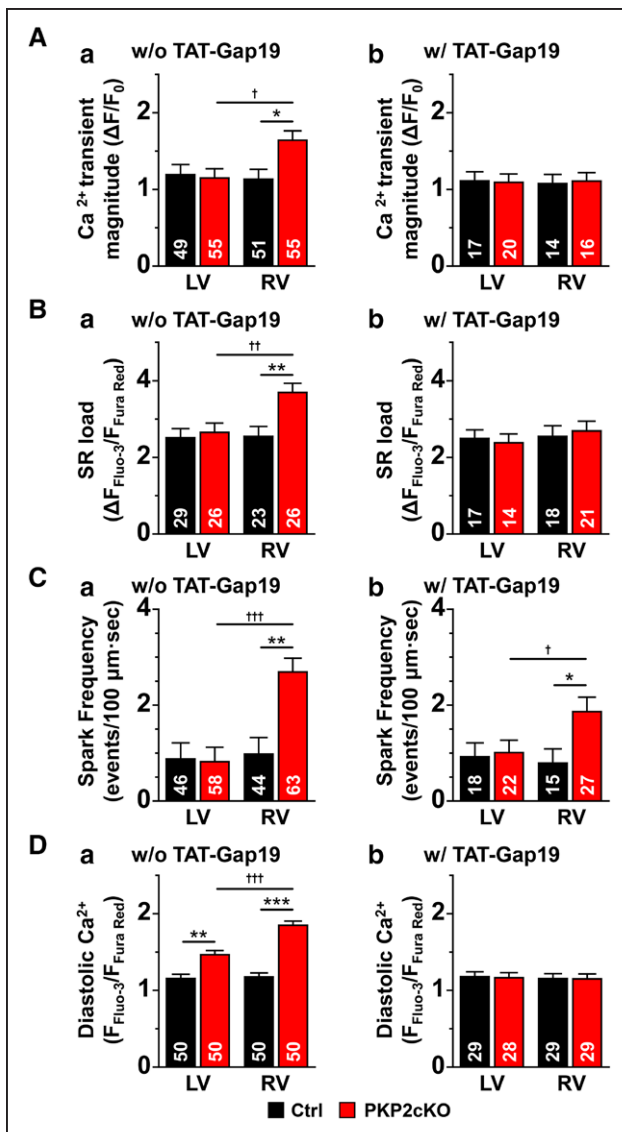


**Figure 8.** Effect of the Connexin 43 (Cx43) hemichannel blocker transactivator of transcription (TAT)-Gap19 on intracellular calcium homeostasis in plakophilin-2 conditional knockout (PKP2cKO) mice.

The left side of **A** through **D** reproduces data presented in previous figures for comparison. TAT-Gap19 (**b**) normalized the increased  $Ca^{2+}$  transient magnitude (relative transient amplitude), sarcoplasmic reticulum (SR) load, and elevated diastolic  $Ca^{2+}$  and reduced the spark frequency toward values similar to those measured in myocytes of PKP2cKO-left ventricle (LV) and in controls. Statistical analysis in right panels: 2-way repeated-measures ANOVA-Bonferroni for  $Ca^{2+}$  transients, SR load, and diastolic  $Ca^{2+}$ . Hierarchical analysis for  $Ca^{2+}$  spark frequency. \* $P < 0.05$  vs control; † $P < 0.05$  vs LV.  $n = 3$  mice. Numbers in columns indicate number of cells tested.

cy toward reduced density in PKP2cKO-RV when compared with control, and separation from the adhesive complex, marked by N-Cadherin localization (see [Figure XIX in the online-only Data Supplement](#)).<sup>33</sup> These data were in agreement with previous studies indicating dislodgment from PKC at the cell junction after loss of mechanical junction integrity.<sup>2</sup> Furthermore, consistent with the loss of a molecule of the adhesion complex (PKP2), ultrastructural analysis of intercalated disc of PKP2cKO RV tissue showed widening of the intercel-

lular space when compared with an RV sample from a control mouse ([Figure XX and Movies I and II in the online-only Data Supplement](#)).

### Enhanced Susceptibility to Arrhythmias in PKP2cKO Hearts

The results presented above led us to examine the arrhythmia susceptibility of PKP2cKO hearts at 14 days post-TAM. As shown in [Figure XXI in the online-only Data Supplement](#), a rapid pace protocol in isoproterenol-exposed Langendorff-perfused hearts led to long runs of ventricular tachycardia in PKP2cKO animals. A similar protocol failed to induce arrhythmias in hearts from control littermates.

## DISCUSSION

Previously, we showed that PKP2cKO mice develop an arrhythmogenic cardiomyopathy of RV predominance 21 days post-TAM injection.<sup>3</sup> To understand its cellular/molecular substrates, here we studied these mice at a time preceding the overt phenotype (ie, 14 days post-TAM) and looked for side-specific differences (RV vs LV). Given our previous data,<sup>3</sup> and given that the phenotype once apparent is both structural and electrical, we focused on a cellular function at the center of both excitability and contraction, namely, regulation of  $[Ca^{2+}]_i$ .

At 14 days post-TAM mice did not show cardiac fibrosis, cellular dimensions were similar to those in control, and left ventricular ejection fraction was within normal limits. Transcriptome differences were minor and levels of PKP2 were drastically down in both ventricles. Yet, we detected important differences in  $[Ca^{2+}]_i$  handling in PKP2cKO RV myocytes, while PKP2cKO LV myocytes remained similar to control. These differences were sensitive to Cx43 reduced expression or Cx43 hemichannel block, and coincided with a Cx43-dependent increase in membrane permeability of the RV, an RV-selective increase in  $[Ca^{2+}]_i$  sensitivity of RyR2, and an RV-selective phosphorylation of RyR2-Thr2809, an amino acid within the phosphorylation hotspot of RyR2 long known to modulate channel gating. The eagerness of RyR2 to trigger  $Ca^{2+}$  sparks was tempered by exposing cells to PKC inhibitors. Based on previous knowledge about: a) the relation between  $[Ca^{2+}]_i$  alterations and arrhythmia susceptibility, b) the importance of regional heterogeneity on arrhythmia generation, and c) the relation between  $[Ca^{2+}]_i$  and cardiac remodeling,<sup>34,35</sup> we propose that  $[Ca^{2+}]_i$  overload and RyR2 dysfunction play a central role in the generation of the electrical and RV-predominant structural phenotype in PKP2-deficient mice.

The Cx43-dependent increase in membrane permeability reported here can explain the excess  $[Ca^{2+}]_i$ . We speculate that PKP2 deficiency causes an excess of “orphan” Cx43 membrane hemichannels that can act as

conduits for Ca<sup>2+</sup> entry. Gap junction plaque formation is known to depend on proper intercellular adhesion.<sup>27</sup> It is also known that Cx43 hemichannels reside in the perimeter of the gap junctions (the perinexus)<sup>36</sup> and are capable, when undocked and in the membrane, to flicker with very low probability.<sup>37,38</sup> Further supporting the relation between PKP2 expression and Cx43-dependent permeable conduits is a recent study showing that PKP2 deficiency can increase cell membrane permeability to ATP, an event prevented by silencing Cx43 expression.<sup>39</sup> We postulate that loss of PKP2 expression, perhaps via weakened intercellular adhesion consequent to loss of desmosomal integrity, causes an increased population of orphan, flickering, Cx43 hemichannels that allow for excess entry of Ca<sup>2+</sup> into the cell. It is worth noting that studies in cell culture systems and in human tissue from ARVC-affected patients have consistently reported that loss of expression or mutations in PKP2 can alter the structure and function of gap junctions.<sup>40–42</sup> We did not detect changes in Cx43 abundance or in gap junction structure, suggesting that functional dysregulation of Cx43 hemichannel activity, coincident with nanostructural changes in the intercalated disc, are among the earliest events following loss of PKP2 expression.

We found increased Ca<sup>2+</sup> sparks frequency in PKP2cKO-RV myocytes. In addition to increased SR Ca<sup>2+</sup> load and higher diastolic [Ca<sup>2+</sup>]<sub>i</sub>, this result may associate with increased sensitivity of RyR2 to Ca<sup>2+</sup>, as well as a change in the phosphorylation state of RyR2-T2809. This residue is located near serine residues well studied as PKA and CAMKII substrates that, when phosphorylated, modify RyR2 gating behavior.<sup>20</sup> We do not know the kinase phosphorylating T2809; however, sequence analysis and data showing that PKC inhibitors reduced Ca<sup>2+</sup> sparks frequency at comparable levels of SR load support the hypothesis of PKC involvement. Interestingly, previous work has shown that PKP2 is necessary to recruit and retain PKC at the desmosome, and that loss of desmosomal integrity releases PKC, freeing it to phosphorylate unintended targets.<sup>2</sup> Consistent with this notion, our single-molecule localization microscopy data indicated reduced phospho-PKC cluster size and density at cell end, and increased phospho-PKC distance from N-Cadherin, a marker of localization of the adhesion complex. Yet, whether phosphorylation of RyR2 in PKP2cKO-RV myocytes is a determinant of RyR2 calcium release remains to be defined.

We observed that SERCA2a protein (but not transcript) levels were decreased, primarily in RV. The latter may play a role in the prolongation of the time constant of recovery in the Ca<sup>2+</sup> transients. Moreover, we saw no difference in NCX function at fixed [Ca<sup>2+</sup>]<sub>i</sub>, though dynamic changes may occur. It is known that Cx43 hemichannels allow for entry not only of Ca<sup>2+</sup> but also Na<sup>+</sup>. Increased [Na<sup>+</sup>]<sub>i</sub> would retard the forward mode activity of the Na<sup>+</sup>-Ca<sup>2+</sup> exchanger, further favoring Ca<sup>2+</sup>

accumulation in the intracellular space. Overall, the activity of NCX to extrude Ca<sup>2+</sup> would be outmatched by persistent intake of external Ca<sup>2+</sup> (and perhaps, Na<sup>+</sup>) through Cx43 hemichannels, reaching a steady-state at higher levels of [Ca<sup>2+</sup>]<sub>i</sub>; this imbalance (or new balance) would be corrected by inhibition or ablation of Cx43. In terms of the relation between RyR2 abundance and function, reduced RyR2 levels may be compensated by the organization of RyR2 units into super-clusters that facilitate calcium release.<sup>11–13</sup> The latter change was not asymmetric, indicating that it may be a substrate that facilitates but is not sufficient to alter Ca<sup>2+</sup> release.

Previous echocardiographic analysis at 14 days post-TAM showed increased RV area in PKP2cKO hearts, an early sign of changes in RV contractility.<sup>3</sup> Partial ablation of Cx43 mitigated this event, likely through normalization of [Ca<sup>2+</sup>]<sub>i</sub>; whether contractile dysfunction is consequent to Ca<sup>2+</sup> dysregulation remains to be determined, though an association between Ca<sup>2+</sup> homeostasis and contractility is well documented.<sup>43</sup> Alternatively, we speculate that the increased RV area is an early manifestation of impaired mechanical forces at the cellular level, combined with the differences in force distribution in various areas of the heart. At the cell level, Broussard et al have shown that impairing the association of desmosomes with intermediate filaments leads to decreased cell tension and stiffness.<sup>44</sup> One can surmise that at the tissue level, these changes would reflect on a weakened ventricular wall, leading to dilation. While the change in cell stiffness may (or may not) be generalized, the forces impacting the ventricular wall are not evenly distributed throughout the heart; recent studies show, for example, that the thin-walled RV (and in particular the RV outflow tract) is exposed to a particularly high wall shear stress.<sup>45</sup> Along these lines, echocardiographic analysis has documented impaired contractility and stiffness of the RV myocardium prior to LV dysfunction in subclinical ARVC patients that present with no evidence of fibrosis by late enhancement magnetic resonance imaging.<sup>46</sup> The latter observation, all major differences notwithstanding, is consistent with the increased RV area in the 14 day post-TAM mice, which precedes overt fibrosis. At the cellular level, these uneven physical forces may cause the RV cells to be first to separate from each other, allowing increased entry of Ca<sup>2+</sup> that in turn, may further impair the contractile function of the cells. Yet, it is important to recognize the role of Wnt-signalling-dependent embryonic programming as potential substrate for asymmetric differences, particularly in case of desmosomal deficiency.<sup>47</sup>

Altogether, we propose that loss of PKP2 expression occurs in both ventricles but first affects RV desmosomal integrity. Loss of desmosomal integrity triggers 2 relatively unrelated events: a) loss of stability of neighboring gap junctions, with consequent increase in orphan Cx43 hemichannels at the perinexus, and

b) dislodgement of a kinase (likely PKC) from the intercalated disc, which translocates to phosphorylate an off-target substrate (RyR2-T2809), changing RyR2 gating properties. These 2 arms converge to facilitate development of potentially lethal arrhythmias and, as time progresses, alter the transcriptional program of the cells and myocyte integrity, leading to arrhythmogenic cardiomyopathy.

Of note, we acknowledge that the mechanisms of arrhythmias may include additional events not yet detected by our experiments. Though we see cellular events that can be arrhythmogenic, and we do see arrhythmias, we do not argue that the arrhythmias are only and exclusively resulting from  $\text{Ca}^{2+}$  alterations.

We focused on PKP2 because of its importance in cardiac biology. Mutations in PKP2 associate with a pleiotropic disease (ARVC) that presents an electrical phenotype sometimes preceding and sometimes concurrent with a cardiomyopathy. It is worth noting that sudden death is the first disease manifestation in 11% of ARVC probands,<sup>5</sup> and that many ARVC cases present mostly an electrical phenotype while the structural disease is concealed<sup>5-7</sup> or not present.<sup>48</sup> This coincides with the observation in our mice, indicating alterations in  $\text{Ca}^{2+}$  homeostasis well-known as potentially arrhythmogenic<sup>3</sup> as first detectable manifestation, prior to collagen accumulation. It is tempting to speculate that elevation of  $[\text{Ca}^{2+}]_i$  can be a trigger for subsequent structural disease and the modified transcriptional program of the heart. Under that scenario, the elevated  $[\text{Ca}^{2+}]_i$  would exert first an arrhythmogenic effect, followed by changes that take more time to manifest, namely, the transcriptional and structural events. Interestingly, despite the elevated  $[\text{Ca}^{2+}]_i$  we did not detect signs of hypertrophy. This and other observations have led us to postulate the hypothesis (yet to be tested) that loss of PKP2 blunts activation of the transcriptional program necessary for compensatory hypertrophy.

We recognize that weaknesses remain with regard to the mechanisms proposed. We have not studied quantitatively the relation between the Cx43-dependent permeability observed in our tissue preparations (demonstrated by the passage of LY) and the  $[\text{Ca}^{2+}]_i$  as it is measured in the single cells. It is important to note though that experimental conditions differ. In particular, the LY experiment is performed in the absence of external  $\text{Ca}^{2+}$  added. This manipulation allows us to see the increased Cx43-dependent membrane permeability within the time frame of our recordings. But the natural time course of the increased  $[\text{Ca}^{2+}]_i$  as it would occur in the heart, remains to be determined. Also, related to the point above, we lack a quantitative description of the magnitude of the  $\text{Ca}^{2+}$  influx taking into account the limited permeability and the presumably low number of Cx43 hemichannels. In

this regard, it is worth noting the study of John et al.<sup>49</sup> These authors calculated that in a cardiomyocyte, 10 open Cx43 hemichannels producing a 100 pA current at  $-80$  mV would increase  $\text{Na}^+$  influx by 75%. This would still represent a small fraction of a total of  $2.6 \times 10^6$  junctional connexins estimated to be present in the myocyte, and yet the increase in intracellular  $\text{Na}^+$  may favor an increase in  $[\text{Ca}^{2+}]_i$ . The amount of open hemichannels at 1 particular snapshot in time would be minimal, not causing a major impact to the cardiomyocyte membrane potential. Yet, the long-term effect of this Cx43 flickering would be the accumulation of  $\text{Ca}^{2+}$  in the intracellular space. Overall, our data strongly support the notion that a Cx43-dependent membrane conduit is necessary for the increased  $[\text{Ca}^{2+}]_i$  reported; nonetheless, how the various  $\text{Ca}^{2+}$  and  $\text{Na}^+$  fluxes balance, through the various membrane compartments, to yield high  $[\text{Ca}^{2+}]_i$  levels remains to be determined.

While our observations are consistent with those in humans with ARVC, any extrapolation needs to be taken with caution, as it is clear that animal models do not reproduce the conditions of a patient with the disease. This is in fact true for all animal or cellular models of ARVC that have been published, and an obvious consequence of the limitations inherent to the study of a human disease. The significance of our studies is not in having reproduced conditions that lead to human ARVC, but in having studied a molecule that, when mutated, causes the disease. Whether the molecular steps described here occur in human hearts with PKP2 mutations remains undefined. Yet, it is worth mentioning that agents that block release of  $\text{Ca}^{2+}$  through RyR2 channels, such as flecainide, may be a possible combination therapy for ARVC patients,<sup>50</sup> and that recent reports indicate that patients with first diagnosis of CPVT have been later identified as carriers of PKP2 mutations.<sup>48</sup> The relation between ARVC and  $\text{Ca}^{2+}$  mishandling is emphasized by the fact that mutations in phospholamban, a known contributor to  $\text{Ca}^{2+}$  homeostasis, can cause ARVC.<sup>5,7</sup> We show a functional intersection of PKP2 and  $\text{Ca}^{2+}$  homeostasis and propose a model as to the steps by which one event (loss of intercellular adhesion at the intercalated disc) affects another ( $\text{Ca}^{2+}$  release), even though they are functions structurally separate in the myocyte space.

## ARTICLE INFORMATION

Received January 11, 2019; accepted August 7, 2019

The online-only Data Supplement is available with this article at <https://www.ahajournals.org/doi/suppl/10.1161/circulationaha.119.039710>.

## Correspondence

Mario Delmar, MD, PhD, The Leon H. Charney Division of Cardiology, New York University School of Medicine, 435 E 30th St, NSB 707, New York, NY 10016; or Marina Cerrone, MD, The Leon H. Charney Division of Cardiology, New York

University School of Medicine, 435 E 30<sup>th</sup> St, NSB 723H, New York, NY 10016.  
Email mario.delmar@nyumc.org or marina.cerrone@nyumc.org

## Affiliations

The Leon H. Charney Division of Cardiology (J.C.K., M.P.H., M.Z., X.L., C.V., M.C., M.D.), Department of Pathology and Genome Technology Center (A.H., G.E.M.), Department of Pharmacology and Biochemistry (Y.Y., E.R.), and Microscopy Laboratory, Division of Advanced Research Technologies (F.X.L.), New York University School of Medicine. Department of Medicine and Cardiovascular Research Center, University of Wisconsin-Madison School of Medicine and Public Health (F.J.A., H.H.V.). Department of Biomedical Sciences (S.R.M., A.L.), and NNF Center for Protein Research (A.L.), Faculty of Health and Medical Sciences, University of Copenhagen, Denmark. Institut du Thorax, Nouvelle Université a Nantes, INSERM, Nantes Cedex 1, France (J.M.). Laboratory of Physiology, College of Pharmacy, Chungnam National University, Daejeon, South Korea (S.H.W.).

## Acknowledgments

The authors acknowledge the excellent support of Joseph Sall and Chris Petzold for EM sample preparation and image acquisition.

## Sources of Funding

This work was supported by grants RO1 HL134328, RO1 HL136179, RO1 HL145911 and a Fondation Leducq Transatlantic Network (to Dr Delmar), grant 18TPA34230006 (to Dr Cerrone), 19CDA34660208 (to Dr Alvarado) from the American Heart Association, grant 2017R1E1A1A01074504 from the National Research Foundation of Korea (to Dr Kim), grants NIH RO1-HL055438 and RO1-HL134344 (to Dr Valdivia), grant NIH S10 ODO019974 (to Dr Liang), grants DFF-6110-00166 and DFF-4092-00045 from The Danish Council for independent Research and NNF18OC0052844 from The Novo Nordisk Foundation (to Dr Lundby), and an Excellence Scholarship from the Rafael del Pino Foundation (to Dr Pérez-Hernández). The NYU Microscopy shared resource is supported by Cancer Center Grant P30CA016087.

## Disclosures

None.

## REFERENCES

- Chen SN, Gurha P, Lombardi R, Ruggiero A, Willerson JT, Marian AJ. The hippo pathway is activated and is a causal mechanism for adipogenesis in arrhythmic cardiomyopathy. *Circ Res*. 2014;114:454–468. doi: 10.1161/CIRCRESAHA.114.302810
- Bass-Zubek AE, Hobbs RP, Amargo EV, Garcia NJ, Hsieh SN, Chen X, Wahl JK 3<sup>rd</sup>, Denning MF, Green KJ. Plakophilin 2: a critical scaffold for PKC alpha that regulates intercellular junction assembly. *J Cell Biol*. 2008;181:605–613. doi: 10.1083/jcb.200712133
- Cerrone M, Montnath J, Lin X, Zhao YT, Zhang M, Agullo-Pascual E, Leo-Macias A, Alvarado FJ, Dolgalev I, Karathanos TV, et al. Plakophilin-2 is required for transcription of genes that control calcium cycling and cardiac rhythm. *Nat Commun*. 2017;8:106. doi: 10.1038/s41467-017-00127-0
- Dubash AD, Kam CY, Aguado BA, Patel DM, Delmar M, Shea LD, Green KJ. Plakophilin-2 loss promotes TGF-β1/p38 MAPK-dependent fibrotic gene expression in cardiomyocytes. *J Cell Biol*. 2016;212:425–438. doi: 10.1083/jcb.201507018
- Groeneweg JA, Bhonsale A, James CA, te Riele AS, Dooijes D, Tichnell C, Murray B, Wiesfeld AC, Sawant AC, Kassamali B, et al. Clinical presentation, long-term follow-up, and outcomes of 1001 arrhythmic right ventricular dysplasia/cardiomyopathy patients and family members. *Circ Cardiovasc Genet*. 2015;8:437–446. doi: 10.1161/CIRCGENETICS.114.001003
- Delmar M, McKenna WJ. The cardiac desmosome and arrhythmic cardiomyopathies: from gene to disease. *Circ Res*. 2010;107:700–714. doi: 10.1161/CIRCRESAHA.110.223412
- Corrado D, Link MS, Calkins H. Arrhythmic right ventricular cardiomyopathy. *N Engl J Med*. 2017;376:61–72. doi: 10.1056/NEJMra1509267
- Liao Y, Day KH, Damon DN, Duling BR. Endothelial cell-specific knockout of connexin 43 causes hypotension and bradycardia in mice. *Proc Natl Acad Sci U S A*. 2001;98:9989–9994. doi: 10.1073/pnas.171305298
- Hulsmans M, Clauss S, Xiao L, Aguirre AD, King KR, Hanley A, Hucker WJ, Wülfers EM, Seemann G, Courties G, et al. Macrophages facilitate electrical conduction in the heart. *Cell*. 2017;169:510–522.e20. doi: 10.1016/j.cell.2017.03.050
- Takefuji M, Wirth A, Lukasova M, Takefuji S, Boettger T, Braun T, Althoff T, Offermanns S, Wettschureck N. G(13)-mediated signaling pathway is required for pressure overload-induced cardiac remodeling and heart failure. *Circulation*. 2012;126:1972–1982. doi: 10.1161/CIRCULATIONAHA.112.109256
- Macquaide N, Tuan HT, Hotta J, Sempels W, Lenaerts I, Holemans P, Hofkens J, Jafri MS, Willems R, Sipido KR. Ryanodine receptor cluster fragmentation and redistribution in persistent atrial fibrillation enhance calcium release. *Cardiovasc Res*. 2015;108:387–398. doi: 10.1093/cvr/cvv231
- Galice S, Xie Y, Yang Y, Sato D, Bers DM. Size matters: ryanodine receptor cluster size affects arrhythmic sarcoplasmic reticulum calcium release. *J Am Heart Assoc*. 2018;7:e008724. doi: 10.1161/JAHA.118.008724
- Kolstad TR, van den Brink J, MacQuaide N, Lunde PK, Frisk M, Aronsen JM, Norden ES, Cataliotti A, Sjaastad I, Sejersted OM, et al. Ryanodine receptor dispersion disrupts Ca(2+) release in failing cardiac myocytes. *Elife*. 2018;7:e39427. doi: 10.7554/eLife.39427
- Xie Y, Yang Y, Galice S, Bers DM, Sato D. Size matters: ryanodine receptor cluster size heterogeneity potentiates calcium waves. *Biophys J*. 2019;116:530–539. doi: 10.1016/j.bpj.2018.12.017
- Agullo-Pascual E, Lin X, Leo-Macias A, Zhang M, Liang FX, Li Z, Pfenniger A, Lübkemeier I, Keegan S, Fenyö D, et al. Super-resolution imaging reveals that loss of the C-terminus of connexin43 limits microtubule plus-end capture and Nav1.5 localization at the intercalated disc. *Cardiovasc Res*. 2014;104:371–381. doi: 10.1093/cvr/cvu195
- Ullrich ND, Valdivia HH, Niggli E. PKA phosphorylation of cardiac ryanodine receptor modulates SR luminal Ca<sup>2+</sup> sensitivity. *J Mol Cell Cardiol*. 2012;53:33–42. doi: 10.1016/j.yjmcc.2012.03.015
- Liu B, Ho HT, Velez-Cortes F, Lou Q, Valdivia CR, Knollmann BC, Valdivia HH, Gyorke S. Genetic ablation of ryanodine receptor 2 phosphorylation at Ser-2808 aggravates Ca(2+)-dependent cardiomyopathy by exacerbating diastolic Ca<sup>2+</sup> release. *J Physiol*. 2014;592:1957–1973. doi: 10.1113/jphysiol.2013.264689
- Camors E, Valdivia HH. CaMKII regulation of cardiac ryanodine receptors and inositol triphosphate receptors. *Front Pharmacol*. 2014;5:101. doi: 10.3389/fphar.2014.00101
- Lundby A, Rossin EJ, Steffensen AB, Acha MR, Newton-Cheh C, Pfeufer A, Lynch SN, Olesen SP, Brunak S, Ellinor PT, et al; QT Interval International GWAS Consortium (QT-IGC). Annotation of loci from genome-wide association studies using tissue-specific quantitative interaction proteomics. *Nat Methods*. 2014;11:868–874. doi: 10.1038/nmeth.2997
- Yuchi Z, Lau K, Van Petegem F. Disease mutations in the ryanodine receptor central region: crystal structures of a phosphorylation hot spot domain. *Structure*. 2012;20:1201–1211. doi: 10.1016/j.str.2012.04.015
- Rust HL, Thompson PR. Kinase consensus sequences: a breeding ground for crosstalk. *ACS Chem Biol*. 2011;6:881–892. doi: 10.1021/cb200171d
- Peng W, Shen H, Wu J, Guo W, Pan X, Wang R, Chen SR, Yan N. Structural basis for the gating mechanism of the type 2 ryanodine receptor RyR2. *Science*. 2016;354:301. doi: 10.1126/science.aah5324
- Lipp P, Hüser J, Pott L, Niggli E. Subcellular properties of triggered Ca<sup>2+</sup> waves in isolated citrate-loaded guinea-pig atrial myocytes characterized by ratiometric confocal microscopy. *J Physiol*. 1996;497 (Pt 3):599–610. doi: 10.1113/jphysiol.1996.sp021793
- Nilbratt M, Porras O, Marutle A, Hovatta O, Nordberg A. Neurotrophic factors promote cholinergic differentiation in human embryonic stem cell-derived neurons. *J Cell Mol Med*. 2010;14(6B):1476–1484. doi: 10.1111/j.1582-4934.2009.00916.x
- Trollinger DR, Cascio WE, Lemasters JJ. Selective loading of Rhod 2 into mitochondria shows mitochondrial Ca<sup>2+</sup> transients during the contractile cycle in adult rabbit cardiac myocytes. *Biochem Biophys Res Commun*. 1997;236:738–742. doi: 10.1006/bbrc.1997.7042
- Kim JC, Wang J, Son MJ, Cuong NM, Woo SH. Sensitization of cardiac Ca<sup>2+</sup> release sites by protein kinase C signaling: evidence from action of murrayafoline A. *Pflugers Arch*. 2015;467:1607–1621. doi: 10.1007/s00424-014-1589-9
- Kostin S, Hein S, Bauer EP, Schaper J. Spatiotemporal development and distribution of intercellular junctions in adult rat cardiomyocytes in culture. *Circ Res*. 1999;85:154–167. doi: 10.1161/01.res.85.2.154
- Danik SB, Liu F, Zhang J, Suk HJ, Morley GE, Fishman GI, Gutstein DE. Modulation of cardiac gap junction expression and arrhythmic susceptibility. *Circ Res*. 2004;95:1035–1041. doi: 10.1161/01.RES.0000148664.33695.2a

29. Gutstein DE, Morley GE, Tamaddon H, Vaidya D, Schneider MD, Chen J, Chien KR, Stuhlmann H, Fishman GI. Conduction slowing and sudden arrhythmic death in mice with cardiac-restricted inactivation of connexin43. *Circ Res*. 2001;88:333–339. doi: 10.1161/01.res.88.3.333
30. Eckardt D, Theis M, Degen J, Ott T, van Rijen HV, Kirchhoff S, Kim JS, de Bakker JM, Willecke K. Functional role of connexin43 gap junction channels in adult mouse heart assessed by inducible gene deletion. *J Mol Cell Cardiol*. 2004;36:101–110. doi: 10.1016/j.yjmcc.2003.10.006
31. Wang N, De Vuyst E, Ponsaerts R, Boengler K, Palacios-Prado N, Wauman J, Lai CP, De Bock M, Decrock E, Bol M, et al. Selective inhibition of Cx43 hemichannels by Gap19 and its impact on myocardial ischemia/reperfusion injury. *Basic Res Cardiol*. 2013;108:309. doi: 10.1007/s00395-012-0309-x
32. Gadicherla AK, Wang N, Bulic M, Agullo-Pascual E, Lissoni A, De Smet M, Delmar M, Bultynck G, Krysko DV, Camara A, et al. Mitochondrial Cx43 hemichannels contribute to mitochondrial calcium entry and cell death in the heart. *Basic Res Cardiol*. 2017;112:27. doi: 10.1007/s00395-017-0618-1
33. Cerrone M, Lin X, Zhang M, Agullo-Pascual E, Pfenniger A, Chkourko Guskys H, Novelli V, Kim C, Tirasawadichai T, Judge DP, et al. Missense mutations in plakophilin-2 cause sodium current deficit and associate with a Brugada syndrome phenotype. *Circulation*. 2014;129:1092–1103. doi: 10.1161/CIRCULATIONAHA.113.003077
34. van Berlo JH, Maillat M, Molkentin JD. Signaling effectors underlying pathologic growth and remodeling of the heart. *J Clin Invest*. 2013;123:37–45. doi: 10.1172/JCI62839
35. Gómez AM, Ruiz-Hurtado G, Benitah JP, Domínguez-Rodríguez A. Ca(2+) fluxes involvement in gene expression during cardiac hypertrophy. *Curr Vasc Pharmacol*. 2013;11:497–506. doi: 10.2174/1570161111311040013
36. Rhett JM, Jourdan J, Gourdie RG. Connexin 43 connexon to gap junction transition is regulated by zonula occludens-1. *Mol Biol Cell*. 2011;22:1516–1528. doi: 10.1091/mbc.E10-06-0548
37. Verma V, Hallett MB, Leybaert L, Martin PE, Evans WH. Perturbing plasma membrane hemichannels attenuates calcium signalling in cardiac cells and HeLa cells expressing connexins. *Eur J Cell Biol*. 2009;88:79–90. doi: 10.1016/j.ejcb.2008.08.005
38. Contreras JE, Sáez JC, Bukauskas FF, Bennett MV. Gating and regulation of connexin 43 (Cx43) hemichannels. *Proc Natl Acad Sci U S A*. 2003;100:11388–11393. doi: 10.1073/pnas.1434298100
39. Cerrone M, van Opbergen CJM, Malkani K, Irrera N, Zhang M, Van Veen TAB, Cronstein B, Delmar M. Blockade of the adenosine 2A receptor mitigates the cardiomyopathy induced by loss of plakophilin-2 expression. *Front Physiol*. 2018;9:1750. doi: 10.3389/fphys.2018.01750
40. Saffitz JE. Arrhythmogenic cardiomyopathy and abnormalities of cell-to-cell coupling. *Heart Rhythm*. 2009;6(8 Suppl):S62–S65. doi: 10.1016/j.hrthm.2009.03.003
41. Asimaki A, Saffitz JE. Remodeling of cell-cell junctions in arrhythmogenic cardiomyopathy. *Cell Commun Adhes*. 2014;21:13–23. doi: 10.3109/15419061.2013.876016
42. Oxford EM, Musa H, Maass K, Coombs W, Taffet SM, Delmar M. Connexin43 remodeling caused by inhibition of plakophilin-2 expression in cardiac cells. *Circ Res*. 2007;101:703–711. doi: 10.1161/CIRCRESAHA.107.154252
43. Eisner DA, Caldwell JL, Kistamás K, Trafford AW. Calcium and Excitation-Contraction Coupling in the Heart. *Circ Res*. 2017;121:181–195. doi: 10.1161/CIRCRESAHA.117.310230
44. Broussard JA, Yang R, Huang C, Nathamgari SSP, Beese AM, Godsel LM, Hegazy MH, Lee S, Zhou F, Sniadecki NJ, et al. The desmoplakin-intermediate filament linkage regulates cell mechanics. *Mol Biol Cell*. 2017;28:3156–3164. doi: 10.1091/mbc.E16-07-0520
45. Gülan U, Saguner AM, Akdis D, Gotschy A, Tanner FC, Kozerke S, Manka R, Brunckhorst C, Holzner M, Duru F. Hemodynamic changes in the right ventricle induced by variations of cardiac output: a possible mechanism for arrhythmia occurrence in the outflow tract. *Sci Rep*. 2019;9:100. doi: 10.1038/s41598-018-36614-7
46. Mast TP, Teske AJ, Walmsley J, van der Heijden JF, van Es R, Prinzen FW, Delhaas T, van Veen TA, Loh P, Doevendans PA, et al. Right ventricular imaging and computer simulation for electromechanical substrate characterization in arrhythmogenic right ventricular cardiomyopathy. *J Am Coll Cardiol*. 2016;68:2185–2197. doi: 10.1016/j.jacc.2016.08.061
47. Li G, Khandekar A, Yin T, Hicks SC, Guo Q, Takahashi K, Lipovsky CE, Brumback BD, Rao PK, Weinheimer CJ, et al. Differential Wnt-mediated programming and arrhythmogenesis in right versus left ventricles. *J Mol Cell Cardiol*. 2018;123:92–107. doi: 10.1016/j.yjmcc.2018.09.002
48. Tester DJ, Ackerman JP, Giudicessi JR, Ackerman NC, Cerrone M, Delmar M, Ackerman MJ. Plakophilin-2 truncation variants in patients clinically diagnosed with catecholaminergic polymorphic ventricular tachycardia and decedents with exercise-associated autopsy negative sudden unexplained death in the young. *JACC Clin Electrophysiol*. 2019;5:120–127. doi: 10.1016/j.jacep.2018.09.010
49. John SA, Kondo R, Wang SY, Goldhaber JI, Weiss JN. Connexin-43 hemichannels opened by metabolic inhibition. *J Biol Chem*. 1999;274:236–240. doi: 10.1074/jbc.274.1.236
50. Ermakov S, Gerstenfeld EP, Svetlichnaya Y, Scheinman MM. Use of flecainide in combination antiarrhythmic therapy in patients with arrhythmogenic right ventricular cardiomyopathy. *Heart Rhythm*. 2017;14:564–569. doi: 10.1016/j.hrthm.2016.12.010